Available online at www.sciencedirect.com

SciVerse ScienceDirect

Journal of the European Ceramic Society 32 (2012) 1077–1083

www.elsevier.com/locate/jeurceramsoc

New binary $(1-x)Ba(Lu_{1/2}Nb_{1/2})O_3$–$xPbTiO_3$ solid solution with morphotropic phase boundary

Dongquan Shen [a,b], Xiuzhi Li [a], Zujian Wang [a], Ying Liu [a], Chao He [a], Tao Li [a], Xifa Long [a,*]

[a] *Key Laboratory of Optoelectronic Materials Chemistry and Physics, Fujian Institute of Research on the Structure of Matter, Chinese Academy of Sciences, Fujian, Fuzhou 350002, China*

[b] *Graduate University of Chinese Academy of Sciences, Beijing 100049, China*

Received 21 October 2011; received in revised form 14 November 2011; accepted 16 November 2011
Available online 9 December 2011

Abstract

A new ferroelectric solid solution of $(1-x)Ba(Lu_{1/2}Nb_{1/2})O_3$–$xPbTiO_3$ (BLN–PT) ($0 \le x \le 1$) has been synthesized by solid state reactions. Its structure and electric properties have been studied by X-ray diffraction and di-/ferro-electric measurements. Based on the investigation, a partial solid state phase diagram of the binary BLN–PT ceramics system has been established, which exhibits a morphotropic phase boundary (MPB) region in the composition range of $0.64 \le x \le 0.68$. The Curie temperature is measured to be around 250 °C in the vicinity of the MPB region, which is much higher than that of PMNT or PZNT system. The dielectric behavior has been discussed based on Curie-Weiss Law and Lorentz-type quadratic relationship. With increasing PT content, a transformation from relaxor to ferroelectric phase has been demonstrated in the solid solution system.

Keywords: $(1-x)Ba(Lu_{1/2}Nb_{1/2})O_3$–$xPbTiO_3$ solid solution; Morphotropic phase boundary; Dielectric, piezoelectric and ferroelectric properties

1. Introduction

Recently much attention has been paid to search for new perovskite-type ferroelectric materials with morphotropic phase boundary (MPB) region because of their promising application in electronics, micro-electronics, ultra-sonic transduction and acoustic sensing.[1–3] Generally, the outstanding piezoelectric and dielectric properties occur in compositions close to the MPB region. The physics and chemistry of the MPB region have been widely studied in the past few years.[4–6] The mechanism of the properties enhancement is to be related with easy paths for polarization rotation in anisotropically flattened free energy profile. Polarization rotation can be switched susceptibly to an electric field drive, making the materials more electrically active, thereby exhibiting the high piezoelectric properties.

Among the lead-based complex pervoskites, taking lead magnesium niobate–lead tianate $Pb(Mg_{1/3}Nb_{2/3})O_3$–$xPbTiO_3$(PMNT) and lead zinc niobate–lead tianate $Pb(Zn_{1/3}Nb_{2/3})$–$xPbTiO_3$(PZNT) as representatives, have attracted much attention due to their superior piezoelectric properties.[7–9] However, there are some major drawbacks in these two systems which limit their application: (1) the Curie temperature(T_C) in the vicinity of the MPB (<170 °C) region is relatively low and especially the lower depoling temperature (60–80 °C) limited their applications at high temperature range.[10–12] (2) High lead content of these ferroelectric materials restricted the usage due to ecological reason. Elimination of such issues has become a driving force for developing lead-free or lead-reduced ferroelectric materials with high Curie temperature and MPB region. Based on this consideration, we recently studied several new lead-reduced ferroelectric solid solutions such as $Ba(Mg_{1/3}Nb_{2/3})O_3$–$xPbTiO_3$,[13] $Ba(Zn_{1/3}Nb_{2/3})O_3$–$xPbTiO_3$,[14] $Ba(Yb_{1/2}Nb_{1/2})O_3$–$xPbTiO_3$[15] and $(1-x)Ba(Sc_{1/2}Nb_{1/2})O_3$–$xPbTiO_3$,[16] and found that all of these systems exhibit a MPB region with the variation of PT content and the best piezoelectric properties always present in MPB region. In this paper, we report the synthesis, phase analysis, dielectric, ferroelectric and piezoelectric properties of another new ferroelectric $(1-x)Ba(Lu_{1/2}Nb_{1/2})O_3$–$xPbTiO_3$ (BLN–PT) solid solution.

* Corresponding author.
E-mail address: lxf@fjirsm.ac.cn (X. Long).

0955-2219/$ – see front matter © 2011 Elsevier Ltd. All rights reserved.
doi:10.1016/j.jeurceramsoc.2011.11.019

2. Experimental procedure

The binary system $(1-x)$BLN–xPT ceramics were synthesized via solid state reactions method with compositions of $x=0$, 0.1, 0.3, 0.5, 0.6, 0.62, 0.64, 0.65, 0.66, 0.67, 0.68, 0.69, 0.7, 0.8 and 1. A two-step calcining technique was used to make the samples. First, the single-phase lutetium niobate ($LuNbO_4$) powder was prepared by mixing starting materials lutetium oxide (Lu_2O_3) (99.9% purity) and niobium oxide (Nb_2O_5) (99.9% purity) powder with ball-milling for 12 h. The mixed powders were then calcined at 1250 °C for 1 h with heating and cooling rates of 10 °C/min. The $LuNbO_4$ powders were subsequently ball-milled with the PbO (99.9% purity), $BaCO_3$ (99.9% purity) and TiO_2 (99.9% purity) for 12 h. At last, the mixed powders of desired compositions were calcined at temperature ranging from 950 °C to 1050 °C for 4 h and sintered at 1200 °C–1500 °C (rate = 5 °C/min).

The phase and morphologies of sintered samples were determined by X-ray diffraction analysis using Cu-Kα radiation (DMAX2500, Rigaku, Japan) and scanning electron microscope (SEM, JSM-6700F, Japan). The density of the sintered samples was measured by the Archimedes method. The sample plates were coated with silver paste as electrodes for electric properties measurements. The dielectric properties were measured by computer-controlled Alpha-broadband dielectric/impedance spectrometer (Novolcontrol GmbH) with an AC signal of 1.0 V (peak-to-peak) applied. The measurements were carried out as a function of temperature upon heating from −50 °C to 350 °C. The ferroelectric properties were measured by aixACCT TF Analyzer 2000 standard ferroelectric test system. A quasi-static d_{33} meter (Model: ZJ-4AN meter, Institute of Acoustics, Chinese Academy of Sciences) was used to measure the piezoelectric coefficients d_{33}.

3. Results and discussion

3.1. Structural analysis

Fig. 1 shows the X-ray diffraction (XRD) patterns for $(1-x)$BLN–xPT ceramics with compositions of $x=0$–0.8. It can be seen that all the samples with different compositions ($x=0.3$–0.8) show pure perovskite structure. The compositions with $x=0$ and $x=0.1$ exhibit super-lattice peaks (as shown in Fig. 2). The absence of anomaly on their dielectric spectra from −150 °C to 200 °C suggests a paraelectric perovskite phase. Therefore we believe that the nature of the super-lattice arises from long range order of Lu^{3+} and Nb^{3+} cations on B-sites of the perovskite structure instead of antiparallel cation displacements. Based on the data of X-ray diffraction, the super-lattice peaks were indexed into (1 1 1), (3 1 1), (3 3 1) and (5 1 1) respectively, marked by small squares in Fig. 2. Hence at room temperature pure BLN and $(1-x)$BLN–xPT with small x ($x \leq 0.1$) ceramic should belong to para-electric phase and have an ordered pervovskite structure with an effective doubling i of unit cell ($2a_c \times 2a_c \times 2a_c$) in relation to the conventional cubic perovskite cell ($a_c \times a_c \times a_c$) with one ABO_3 formula unit per unit cell. The main feature of these XRD patterns is the evolution of the (2 0 0) peak with the variation of PT content, which shows the rhombohedral symmetry when $x<0.64$ and split into two peaks of (0 0 2)/(2 0 0) when $x>0.68$, indicating the presence of tetragonal phase. For $x=0.64$ to $x=0.68$, the (2 0 0) peaks first become broadened and asymmetrical and then split at $x=0.69$, suggesting that the symmetry of the phase gradually changes from rhombohedral to tetragonal upon increasing PT content from $x=0.64$ to $x=0.68$, where the rhombohedral and tetragonal phase coexist in this range. Therefore, a morphotropic phase boundary (MPB) region was demonstrated between $x=0.64$ and $x=0.68$.

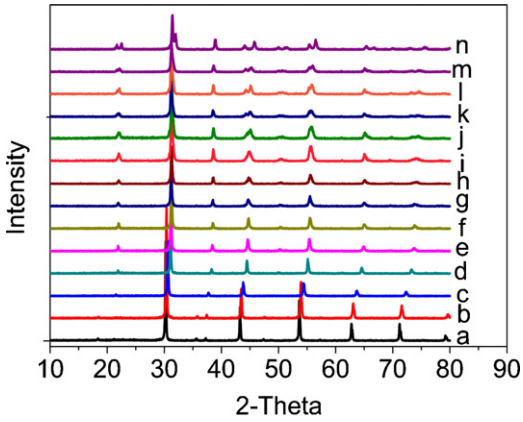

Fig. 1. X-ray diffraction patterns of the $(1-x)$BLN–xPT ceramics at room temperature ((a) $x=0$, (b) $x=0.1$, (c) $x=0.3$, (d) $x=0.5$, (e) $x=0.6$, (f) $x=0.62$, (g) $x=0.64$, (h) $x=0.65$, (i) $x=0.66$, (j) $x=0.67$, (k) $x=0.68$, (l) $x=0.69$, (m) $x=0.7$ and (n) $x=0.8$).

Fig. 3 shows some selected experimental XRD data (shown in open circles) of the pseudo-cubic (2 0 0) reflection for the compositions of $x=0.62$, 0.66, and 0.69. The peak profile is deconvoluted with the tetragonal and/or rhombohedral phase components. It can be seen that the (2 0 0) reflection of the composition with $x=0.62$ and $x=0.69$ are composed of one single peak and two distinct peaks, corresponding to the rhombohedral and tetragonal phase respectively. For $x=0.66$, the peak profile can be fitted into three peaks. The dominant broad peak 1 corresponds to the rhombohedral phase and the weak peaks 2 and

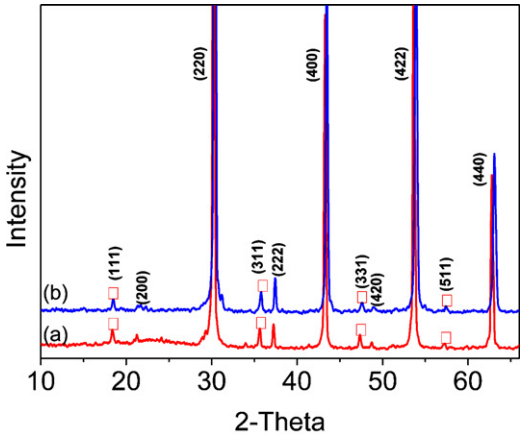

Fig. 2. X-ray diffraction patterns and super-lattice reflections for $(1-x)$BLN–xPT ceramics ($x=0$ and 0.1), marked as square symbol.

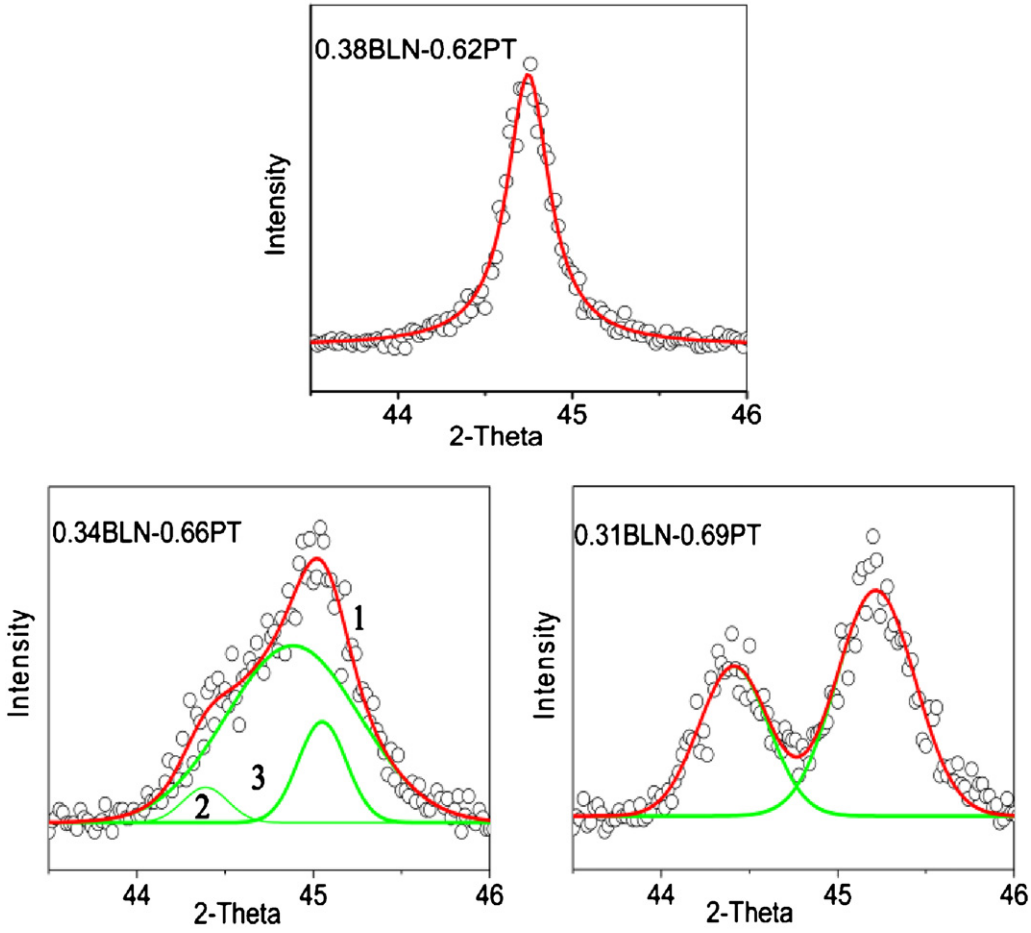

Fig. 3. Pseu-cubic (2 0 0) reflection (open circles) of $(1-x)$BLN–xPT with the composition of $x=0.62$, $x=0.66$ and $x=0.69$ at room temperature. Among these composition $x=0.62$ and $x=0.69$ are respectively fitted to the rhombohedral phase and tetragonal phase, while $x=0.66$ mixes the two phases.

3 arising from the tetragonal phase. The phase analysis further confirms that the coexistence of the rhombohedral and tetragonal phases.

The SEM micrographs of the fracture of surface for $(1-x)$BLN–xPT are shown in the Fig. 4. The grain sizes and the density measuring results for some selected samples are listed in the Table 1. It can be seen that all samples are highly dense and the grain size is in the ranges of 500 nm–2 μm, changing slightly with increasing PT content.

3.2. Dielectric properties and phase transitions

Fig. 5 shows the dielectric constant as a function of temperature at frequencies $f=10$ Hz, 100 Hz, 1 kHz and 10 kHz for the selected compositions of $x=0$, 0.5, 0.6, and 0.7 as examples. For $x=0$, pure BLN is of cubic symmetry and has no obvious peak in the temperature range from −150 °C to 200 °C, indicating no any phase transition occurs in this temperature range. For $x=0.5$ and $x=0.6$, the dielectric spectra present broad maximum shifting to higher temperature with increasing frequency, showing typical relaxor behavior. For $x=0.7$, the peaks become sharper and independent of frequency, indicating a normal ferroelectric behavior. Therefore, $(1-x)$BLN–xPT solid solution shows clear transition from typical relaxor to normal ferroelectrics system with increasing PT content.

The dielectric characterization of relaxor ferroelectric materials are known to deviate from Curie-Weiss (CW) law and can be described by a Lorentz-type quadratic relationship, given by[17–20]:

$$\frac{\varepsilon_A}{\varepsilon'} - 1 = \frac{(T-T_A)^2}{2\delta^2} \quad (1)$$

where T_A and ε_A are the fitting parameters and δ is a measure of diffuseness of the permittivity peak. Fig. 6 shows the $1/\varepsilon'$ as a function temperature at 1 kHz for the 0.5BLN–0.5PT ceramics as a example. When temperature is above Burns temperature ($T_B=471$ K), the dielectric constant follows CW law: $1/\varepsilon'=(T-T_o)/C$, where T_o is the Curie-Weiss temperature and C is the Curie constant. The parameters are obtained from the linear fit above T_B with $C=1.59\times10^5$ and $T_o=226$ K. However, with decreasing temperature, dielectric constant deviates from CW law in a wide range temperature ($T_m<T<T_B$) because of the existence and interaction of polar nanoregions (PNRs).[21] The inset of the Fig. 6 shows the $1/\varepsilon'$ as a function of temperature

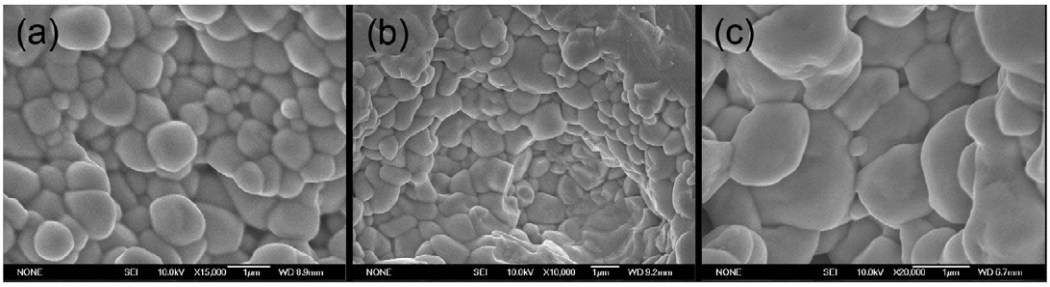

Fig. 4. SEM micrographs of the fracture surface for $(1-x)$BLN–xPT: (a) $x=0.6$, (b) $x=0.68$ and (c) $x=0.7$.

Table 1
Comparison of grain size, density and electric properties for $(1-x)$BLN–xPT binary ceramics with different compositions (G, average grain size; ρ, density; ρ_r, relative density; T_B, Burns temperature at 1 kHz; T_m, maximum temperature at 100 kHz; ε', dielectric constant at room temperature; E_C, coercive field).

Compositions	G (μm)	ρ (g/cm^3)	ρ_r (%)	T_B (k)	T_m (°C)	ε'@RT	E_c (kV/cm)
0.70BLN–0.30PT	1.1	7.70	97.7	–	–	200	–
0.50BLN–0.50PT	0.8	7.68	98.5	471	−50	990	–
0.40BLN–0.60PT	1.0	7.53	97.1	503	90	1925	2.8
0.34BLN–0.66PT	1.0	7.51	97.1	542	210	904	23
0.32BLN–0.68PT	1.1	7.62	98.6	578	250	1021	27
0.20BLN–0.80PT	1.3	7.58	98.7	676	380	400	52

starting from a few degrees below T_m, which is fitted into quadratic relation [Eq. (1)] with the parameters of $T_A=243$ K, $\varepsilon_A=1008.76$ and $\delta=212.4$ K. Similarly, the T_B and T_m for several selected samples have been estimated and listed in the Table 1, which shows that the T_B and T_m increase gradually with the increasing PT content.

The temperature dependence of the dielectric constant (at 100 kHz) as a function of composition is displayed in the Fig. 7. The compositions with $x=0.5$–0.69 show broad peaks which correspond to ferroelectric–paraelectric phase transition. With increasing PT content, the phase transition temperature increases and reaches a value of 250 °C for the composition $x=0.68$

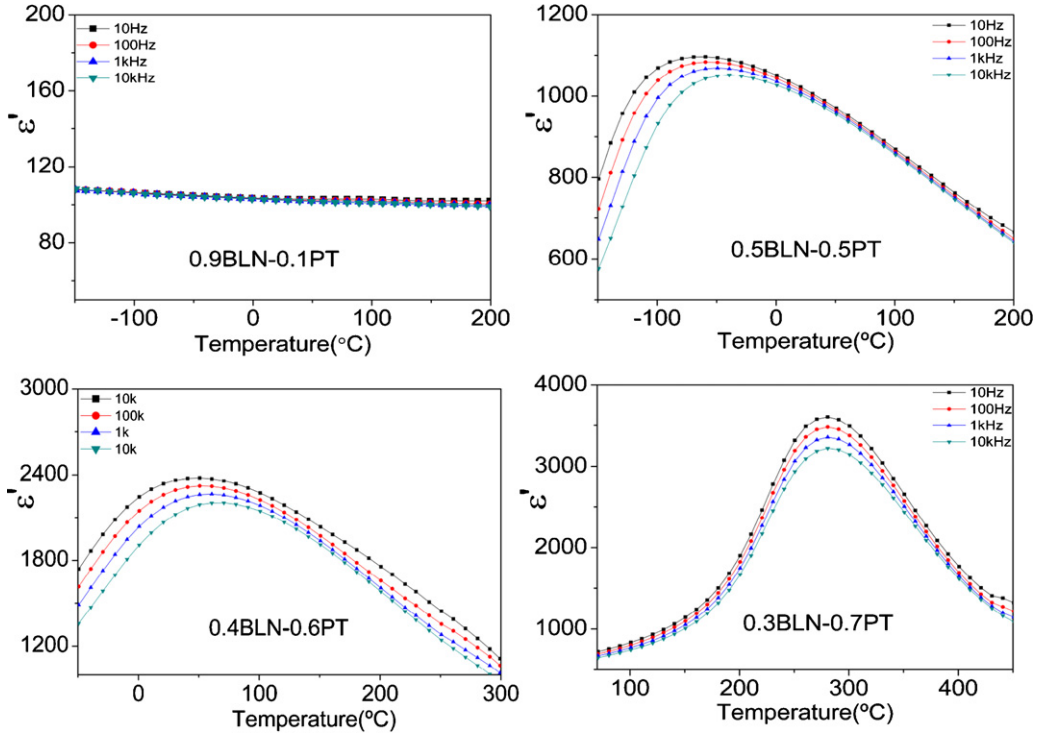

Fig. 5. Variations of the dielectric constant ε' as a function of temperature for BLN, 0.5BLN–0.5PT, 0.4BLN–0.6PT and 0.3BLN–0.7PT ceramics at the frequencies of $f=10$ Hz, 100 Hz, 1 kHz and 10 kHz.

Table 2
Electric properties of lead-reduced BMeN–PT(Me: Mg, Zn, Yb, Sc and Lu) MPB piezoelectric ceramics.

Compositions	MPB (% PT)	P_r (μC/cm^2)	d_{33} (pC/N)	T_C (°C)	ε'@RT	Ref.
0.3BMN–0.7PT	71–79	10	118	230	700	13
0.37BZN–0.63PT	58–61	10	125	55	4000	14
0.32BYN–0.68PT	65–70	17	100	200	800	15
0.37BSN–0.63PT	61–66	11	120	120	800	16
0.32BLN–0.68PT	64–68	18.5	150	250	1000	This work

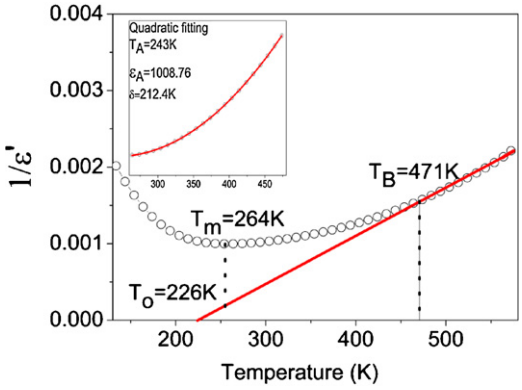

Fig. 6. $1/\varepsilon'$ as a function of temperature at 1 kHz for the 0.5BLN–0.5PT ceramic. Solid line is fitting to the Curie-Weiss law. Inset is the fit to the Lorentz-type quadratic relationship from 252 K to 473 K.

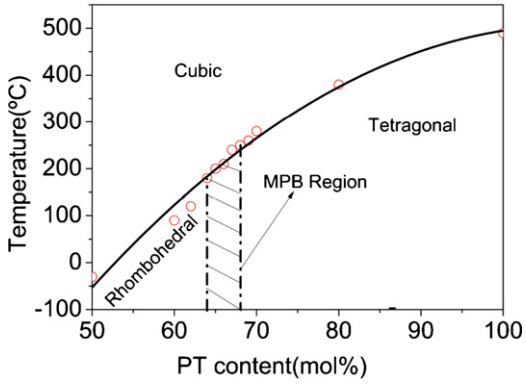

Fig. 8. Partial phase diagram for $(1-x)$BLN–xPT solid solution ceramics. The top line represents paraelectric-to-ferroelectric phase transitions (obtained by dielectric peak at 100 kHz). The MPB region is obtained by XRD.

within the MPB region. Compared with the BYN–PT, BSN–PT, BMN–PT and BZN–PT solid solutions, the phase transition temperature T_C is enhanced within the MPB region (as listed in Table 2).

3.3. Phase diagram

Based on the XRD and dielectric measurements results at 100 kHz, a T–x phase diagram of the $(1-x)$BLN–xPT binary system with the composition $x=0.5$–0.8 are established, as shown in Fig. 8. Based on the phase diagram, we can distinguish the regions of paraelectric phase (*Pm3m*), the rhombohedral relaxor phase (*R3m*) and the tetragonal phase (*P4mm*). The morphotropic phase boundary locates in the composition range of $x=0.64$–0.68, where the rhombohedral phase and tetragonal phase coexist.

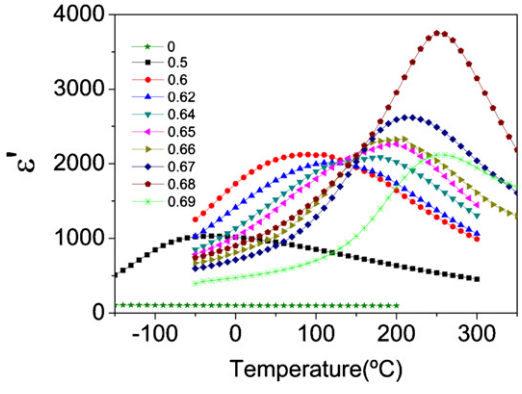

Fig. 7. Dielectric constant as a function of temperature for the $(1-x)$BLN–xPT solid solution ceramics with $x=0$, 0.5, 0.6, 0.62, 0.64, 0.65, 0.66, 0.67, 0.68, 0.69, measured at the frequency of 100 kHz.

3.4. Ferroelectricity

Fig. 9 shows the saturated polarization–electrical field (P–E) hysteresis loops of $(1-x)$BLN–xPT solid solution with compositions of $x=0.5$, 0.6, 0.64, 0.68, 0.69 and 0.7 at room temperature under a maximum applied electric field (E_m) of 80 kV/cm. For compositions of $x\leq 0.5$, a linear P–E relationship is observed without any hysteretic behavior at the room temperature due to the nature of paraelectric phase. For compo-

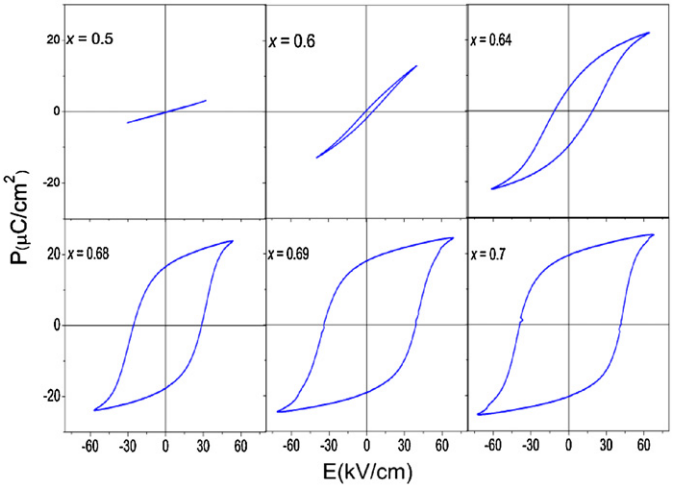

Fig. 9. Polarization–electrical field (P–E) hysteresis loops of $(1-x)$BLN–xPT solid solution with the composition: $x=0.5$, 0.6, 0.64, 0.68, 0.69, 0.7.

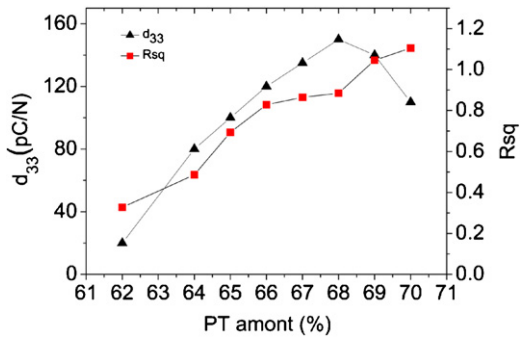

Fig. 10. Piezoelectric coefficient d_{33} and hysteresis loop squareness value R_{sq} for $(1-x)$BLN–xPT solid solution as function of x content.

sitions of $x \geq 0.6$, loops become more and more "square" with increasing PT content. The remnant polarization (P_r) reaches about 20 μC/cm^2 with the coercive field of about 40 kV/cm for the composition $x = 0.7$.

Ferroelectric domain is characterized as a phase containing long-range interaction between dipoles.[22] Therefore a typical "square" form P–E hysteresis loop exist for normal ferroelectrics as a result of domain switching in responds to applied field. The development of a long-range ferroelectric order results in more and more "square" loop of $(1-x)$BLN–xPT ceramics with increasing x. The highly ordered system thus requires stronger field for domain switching, which aligns dipole moment to a point parallel to the field, giving rise to the increase of the coercive field and more "square" of the hysteresis curves.[23] The ferroelectric characteristics of ceramics can be assessed by the hysteresis loop squareness value R_{sq}.[24]

$$R_{sq} = \left(\frac{P_r}{P_s}\right) + \left(\frac{P_{1.1Ec}}{P_r}\right) \quad (3)$$

where P_s is the saturated polarization, $P_{1.1Ec}$ is the polarization of the field equal to $1.1E_C$. For the ideal square loop, R_{sq} is equal to 2. As shown in Fig. 10, the value of R_{sq} increases with increasing PT amount.

3.5. Piezoelectricity

Fig. 10 shows the piezoelectric d_{33} constant as a function of x. It can be seen that the piezoelectric coefficient d_{33} increased with increasing PT content until it reached maximum (150 pC/N) at $x = 0.68$ and slightly decreased as $x \geq 0.69$ at room temperature. The change of d_{33} with the variation of composition demonstrate that the best piezoelectric properties appear within the MPB region. Compare to other lead-reduced $(1-x)$BMeN–xPT ceramics, the d_{33} are slightly improved (as listed in Table 2).

4. Conclusions

A new $(1-x)Ba(Lu_{1/2}Nb_{1/2})O_3$–$xPbTiO_3$ solid solution ceramics has been prepared by solid solution reactions and characterized by X-ray diffraction, dielectric and ferroelectric measurements. Based on the structural and dielectric characterizations, the partial T–x solid state phase diagram of the binary system has been constructed. A morphotropic phase boundary region is found to exist within the composition range of $0.64 < x < 0.68$. Upon increasing PT content, the solid solution displays a spectrum of properties from simple dielectric, to relaxor, and to ferroelectric. The relaxor behavior in the solid solution of 0.5BLN–0.5PT has been discussed by a Lorentz-type quadratic relationship and Curie Weiss law. By introducing squareness value R_{sq}, the trend of hysteresis loop quantitatively has been revealed. The compounds of the MPB compositions exhibit a $T_C > 250\,^{\circ}C$, making the BLN–PT system promising high Curie temperature and lead-reduced materials for potential piezo- and ferro-electric applications.

Acknowledgement

This work was supported by the National Natural Science Foundation of China under Grant No. 91122020, the Fund of Key Projects of Fujian Provincial (2010H0023) and SZD08002.

References

1. Haertling GH. Ferroelectric ceramics: history and technology. *J Am Ceram Soc* 1999;**82**:797–818.
2. Newnham RE, Ruschau GR. Smart electroceramics. *J Am Ceram Soc* 1991;**74**:463–80.
3. Yamashita Y. PZN-based relaxors for MLCCS. *Am Ceram Soc Bull* 1994;**73**:74–80.
4. Ahart M, Somayazulu M, Cohen RE, Ganesh P, Dera P, Mao HK, Hemlev RJ, Ren Y, Liermann P, Wu Z. Origin of morphotropic phase boundaries in ferroelectrics. *Nature* 2008;**451**:545–8.
5. Fu HX, Cohen RE. Polarization rotation mechanical for ultrahigh electromechanical response in single-crystal piezoelectrics. *Nature* 2000;**403**:281–6.
6. Park SE, Shrout TR. Ultrahigh strain and piezoelectric behavior in relaxor based ferroelectric single crystals. *J Appl Phys* 1997;**82**:1804–11.
7. Choi SW, Shrout TR, Jang J, Bhalla AS. Dielectric and pyroelectric properties in the $Pb(Mg_{1/3}Nb_{2/3})O_3$–$PbTiO_3$ system. *Ferroelectrics* 1989;**100**:29–38.
8. Uchino K. High electromechanical coupling piezoelectrics: relaxer and normal ferroelectric solid solutions. *J Solid State Ionics* 1998;**108**:43–52.
9. Dong M, Ye ZG. High-temperature solution growth and characterization of the piezo-/ferroelectric $(1-x)Pb(Mg_{1/3}Nb_{2/3})O_3$–$xPbTiO_3$ [PMNT] single crystals. *J Cryst Growth* 2000;**209**:81–90.
10. Park SE, Hackenberger W. High performance single crystal piezoelectrics: applications and issues. *Curr Opin Solid State Mater* 2002;**6**:11–8.
11. Zhang SJ, Rechrig PW, Randall C, Shrout TR. Crystal growth and electrical properties of $Pb(Yb_{1/2}Nb_{1/2})O_3$–$PbTiO_3$ perovskite single crystals. *J Cryst Growth* 2002;**234**:415–20.
12. Eitel RE, Randall CA, Shrout TR, Rehrig PW, Hackenberger W, Park SE. New high temperature morphotropic phase boundary piezoelectrics based on $Bi(Me)O_3$–$PbTiO_3$ ceramics. *Jpn J Appl Phys* 2001;**40**:5999–6002.
13. Long X, Ye ZG. A new solid solution of $(1-x)Ba(Mg_{1/3}Nb_{2/3})O_3$–$xPbTiO_3$ with dielectric, relaxor and ferroelectric properties. *Chem Mater* 2007;**19**:1285–9.
14. Long X, Ye ZG. Phase diagram, di-/ferroelectirc properties of a new $(1-x)Ba(Zn_{1/3}Nb_{2/3})O_3$–$xPbTiO_3$ solid solution. *J Appl Phys* 2007;**101**:124101.
15. Wang Z, Li X, Wei Q, Long X, Ye ZG. A ferroelectric solid solution of $(1-x)Ba(Yb_{1/2}Nb_{1/2})O_3$–$xPbTiO_3$ with morphotropic phase boundary. *J Appl Phys* 2008;**104**:046102.
16. Wei Q, Wang Z, Li X, Long X, Ye ZG. Morphotropic phase diagram and dielectric and ferroelectric properties of $(1-x)Ba(Sc_{1/2}Nb_{1/2})O_3$–$xPbTiO_3$ solid solution. *Chem Mater* 2009;**21**:506–10.
17. Bokov AA, Ye ZG. Recent progress in relaxor ferroelectrics with perovskite structure. *J Mater Sci* 2006;**41**:31–52.

18. Bokov AA, Bing YH, Chen W, Ye ZG, Bogatina SA, Raevski IP, Raevskaya SI, Sahkar EV. Empirical scaling of the dielectric permittivity peak in relaxor ferroelectrics. *Phys Rev B* 2003;**68**:052102.
19. Bokov AA, Ye ZG. Phenomenological description of dielectric permittivity peak in relaxor ferroelectrics. *Solid State Commun* 2000;**116**: 105–8.
20. Han X, Li X, Long X, Cao Y. A dielectric and ferroelectric solid solution of $(1-x)BaSnO_3$–$xPbTiO_3$ with morphotropic phase boundary. *J Mater Chem* 2009;**19**:6132–6.
21. Smolenskii GA. Physical phenomena in ferroelectrics with diffused phase transition. *J Phys Soc Jpn* 1970;**28**:26–37.
22. Koval V, Alemany C, Briancin J, Brunckova H, Saksl K. Effect of PMN modification on structure and electrical response of xPMN–$(1-x)$PZT ceramic systems. *J Eur Ceram Soc* 2003;**23**:1157–66.
23. George AS. The relaxational properties of compositionally disordered ABO_3 perovskites. *J Phys Condens Matter* 2003;**15**:R367–411.
24. Jin BM, Kim J, Kim SC. Effects of grain size on the electrical properties of $PbZr_{0.52}Ti_{0.48}O_3$ ceramics. *Appl Phys* 1997;**65**:53–6.